Complimentary use of dating and hydrochemical tools to assess mixing processes involving centenarian groundwater in a geologically complex alpine karst aquifer

Keywords: Groundwater dating · Alpine karst · Complex aquifer · Groundwater age distribution · Lumped Parameter Models · Shape-Free Models · Hydrochemistry

Running title: Dating and hydrochemical tools applied to an alpine karst aquifer

Gil-Márquez, José Manuel (*)[1]; De la Torre, Beatriz[1]; Mudarra, Matías[1]; Sültenfuß, Jürgen[2] & Andreo, Bartolomé[1]

(1) Department of Geology and Center of Hydrogeology of the University of Málaga, Facultad de Ciencias, s/n. E-29071, Málaga, Spain. josemgil@uma.es, delatorrem@uma.es, andreo@uma.es, mmudarra@uma.es

(2) Institute of Environmental Physics, University of Bremen, Otto-Hahn-Allee, D-28359 Bremen, Germany. suelten@uni-bremen.de

(*) Corresponding author

Acknowledgments: This work is a contribution of the research group RNM-308 of Junta de Andalucía to the projects CGL2012-32590 and CGL2015-65858R of the General Office of Scientific and Technical Research (DGICYT) of the Spanish Government. The authors thank Klaus Bulsiewicz (the University of Bremen, Institute of Environmental Physics, Department of Oceanography) for running the samples for CFC-12 determinations and helping on its dating interpretation.

Data Availability Statement

The data that support the findings of this study are available from the corresponding author upon reasonable request.

Complimentary use of dating and hydrochemical tools to assess mixing processes involving centenarian groundwater in a geologically complex alpine karst aquifer

Abstract

Environmental dating tracers (^{3}H, ^{3}He, ^{4}He, CFC-12, CFC-11, SF_6) and the natural spring response (hydrochemistry, water temperature, and hydrodynamics) were jointly used to assess mixing processes and to characterize groundwater flow in a relatively small carbonate aquifer with complex geology in southern Spain. Results evidence a marked karst behavior of some temporary outlets, with sharp and rapid responses to precipitation events, while some perennial springs show buffer and delayed variations with respect to recharge periods. The general geochemical evolution shows a pattern, from higher to lower altitudes, in which mineralization and the Mg/Ca ratio rise, evidencing longer water-rock interaction. The large SF_6 concentrations in groundwater suggest terrigenic production, whereas CFC-11 values are affected by sorption or degradation. The groundwater age in the perennial springs —as deduced from CFC-12 and $^{3}H/^{3}He$— points to mean residence times of several decades, although the difference between the two methods and the large amount of radiogenic ^{4}He in samples indicates a contribution of old groundwater (free of ^{3}H and

CFC-12). Lumped Parameter Models and Shape-Free Models were created based on ^{3}H, tritiogenic ^{3}He, CFC-12, and radiogenic ^{4}He data in order to interpret the age distribution of the samples. Results evidence the existence of two mixing components, with an old fraction ranging between 160 and 220 years in age. The correlation of physicochemical parameters with some dating parameters derived from the mixing models serves to explain the hydrogeochemical processes occurring within the system. Altogether, long residence times are shown to be possible in small alpine systems with a clearly karst behavior if the geological setting features highly tectonized media including units with diverse hydrogeological characteristics. These findings highlight the importance of applying different approaches, including groundwater dating techniques, when studying such groundwater flow regimes.

Keywords: Groundwater dating · Alpine karst · Complex aquifer · Groundwater age distribution · Lumped Parameter Models · Shape-Free Models · Binary mixing · Hydrochemistry

1. INTRODUCTION

Environmental tracers are natural or anthropogenic compounds widely distributed in the near-surface of the Earth (Cook & Herczeg, 2000; Elliot, 2014). Determining their concentrations in groundwater helps researchers assess the age of the water and the recharge regime of aquifers (Müller et al., 2016; Wilske et al., 2019; Yager et al., 2010), mixing process problems (Akesson et al., 2015; Corcho Alvarado et al., 2007), as well as

groundwater vulnerability to pollution (Jasechko et al., 2017; Musgrove, Solder, Opsahl, & Wilson, 2019), and can lead to the development of optimized hydrogeological conceptual models (Gardner & Heilweil, 2014; Sültenfuss, Purtschert, & Führböter, 2011).

Groundwater dating based on environmental tracers such as radioactive isotopes (^{3}H, ^{14}C, ^{36}Cl, ^{85}Kr), noble gases isotopes (^{3}He, ^{4}He, ^{40}Ar), and fluorinated synthetic gases (CFCs, SF_6) has been conducted worldwide in recent decades, particularly in detrital formations (Beyerle et al., 1999; Corcho Alvarado et al., 2007; Mayer et al., 2014; Xu, Gong, & Yang, 2018) and fractured bedrock aquifers (Cook, Solomon, Sanford, Busenberg, & Plummer, 1996; Jaunat et al., 2012; Koh et al., 2018). However, groundwater dating based on environmental gas tracers is uncommon in karst hydrogeology, compared to other specific approaches (Goldscheider & Drew, 2007). The interpretation of groundwater ages in karst media is challenging because of the high flow-heterogeneity that can be found in these aquifers. While groundwater flows rapidly through conduits and fractures, the flow velocity in the matrix or small fissures is very slow (Han, Hacker, & Gröning, 2007; Worthington & Gunn, 2009). It calls for the joint application of several environmental tracers to constrain the age distribution of groundwater (Wilske et al., 2019), particularly if a comprehensive understanding of groundwater flow behavior is not derived from other experimental methodologies (hydrodynamic, hydrothermal, hydrochemical, and stable isotopes).

Several studies have demonstrated the applicability of environmental tracers for groundwater dating in karst systems, shedding light on flow dynamics involving recently

infiltrated water and older groundwater components. The latter fraction in the mix may be a few decades old (Delbart et al., 2014; Jiang, Guo, & Tang, 2019), yet more commonly was infiltrated before the middle of the 20th Century, before the anthropogenic release of ^{3}H and CFCs (Han et al., 2007; Long & Putnam, 2009; Toth & Katz, 2006; Yager et al., 2010; Zang, Zheng, Qin, & Jia, 2015). In regional carbonate aquifers, some partially confined, dating old groundwater components can give ages of hundreds or even thousands of years (Land & Huff, 2010; Müller et al., 2016; Musgrove et al., 2019; Plummer, Busby, Lee, & Hanshaw, 1990; Xanke et al., 2015). Karst aquifers in alpine mountains, however, tend to have recently infiltrated (young) groundwater, with a maximum mean recharge rate of a few years, sometimes mixed with a low percentage of older components (Althaus et al., 2009; Rank, Volkl, Maloszewski, & Stichler, 1992; Shah, Jeelani, & Jacob, 2017).

Alpine karst, at a high altitude, is characterized by pronounced relief, intense tectonic deformation implying hydrogeological complexity, and sparse or no vegetal and soil covers (Field, 1999; Palmer, 1984). Major height variations existing in alpine karst generally entail a thick unsaturated zone and high hydraulic gradients, meaning rapid flow and short residence times within the conduit network (Werner, 1979). These characteristics are more marked in small aquifers. Though alpine karst formations are named after the Alps (Central Europe), they can be found all over Europe (Ballesteros, Jiménez-Sánchez, Giralt, García-Sansegundo, & Meléndez-Asensio, 2015; Lauber & Goldscheider, 2014; Mudarra & Andreo, 2011; Turk et al., 2015), Asia (Ebrahimi,

Pasandi, & Ahmadipour, 2007; Shah et al., 2017; Wu et al., 2019), and North America (Ford, 1983; Smart, 1988; Spangler, 2001).

This study highlights the complementarity of conventional hydrogeological tools and groundwater dating techniques for evaluating mixing processes involving components of different ages in geologically complex alpine karst areas. Environmental dating tracer data (^{3}H, $^{3}He_{trit}$, $^{4}He_{rad}$, CFC-12, CFC-11, and SF_6) are considered along with the hydrodynamic, hydrochemical, and groundwater temperature data series from several springs draining a relatively small yet complex alpine karst aquifer (Jarastepar) in southern Spain. Based on the concentration of environmental dating tracers in the samples, Lumped Parameter Models, and Shape-Free Models were created to assess the groundwater age distribution in diverse water conditions. The simultaneous application of different methodologies is a significant and quantitative advance toward hydrogeological knowledge of karst systems. An improved conceptual model —the basis for a numerical model— of aquifer functioning can be thereby be established, more solid than if convetional hydrogeological tools or dating techniques were applied individually. This joint approach can prove useful in particular cases of alpine karst for which conventional hydrogeological methods do not explain the whole complexity of the aquifer.

2. SETTING

The pilot site is located in the central part of the Ronda Mountains, in southern Spain (Fig. 1). The catchment area covers a rugged land surface of 56 km^2 (38 km^2 of carbonate

rocks) with altitudes ranging from 400 to 1400 m a.s.l. and an average slope of 20 %. The climate is Mediterranean type. Mean precipitaiton in the area amounts to 1,050 mm/yr, and rainfall generally occurs between autumn and springtime. The average values of precipitation and temperature recorded at the Jarastepar meteorological station (1,317 m a.s.l.; Fig. 1) during the research period (October 2014 to December 2016) are respectively 770 mm/yr and 12.2 ºC. During recharge times, an average temperature of 8 ºC was recorded.

From a geological standpoint, the research area presents a complex structure that involves rocks from three main tectonic domains of the Betic Cordillera (Figs. 1 & 2):

a) the External Zone (EZ), occupying the lowest tectonic position and lithostratigraphically formed, from the bottom to the top, by Upper Triassic clays and evaporites, Jurassic dolostones and limestones (>500 m thick), and Cretaceous-Tertiary marly-limestones and marls (Martín-Algarra, 1987);

b) the Internal Zone (IZ), overlapping the External Zone from the southwest, with up to 400 m of Paleozoic metamorphic rocks (mainly schists) and more than 1,000 m of carbonate formations (mainly dolostones);

c) the Flysch Complex (FC), formed by Tertiary clays and sandstones, discontinuously imbricated between the two previous domains (defining the tectonic suture).

The geological structure of the EZ is characterized by a NE-SW anticlinorium fold, overthrusting with vergence toward the NW the Triassic clays of the anticline core. Likewise, the internal structure of carbonate formations from the IZ corresponds to the

normal limb of a large ENE-WSW-trending north-verging synform developed eastward of the study area (Martín-Algarra, 1987). The set of geological units is affected by more recent strike-slip faults (NW-SE) and normal fractures (NE-SW and N-S) (Fig. 1).

In hydrogeological terms, the Jarastepar aquifer comprises fractured and karstified Triassic (IZ) and Jurassic (EZ) carbonate rocks bounded by low permeability formations, mainly Triassic clays and Cretaceous-Paleogene marls of the EZ (Fig. 1). However, the southern border coincides with a major tectonic contact between the materials of the EZ and the IZ, involving rocks of very different permeabilities (Fig. 2). Recharge occurs through rainfall infiltration over the carbonate outcrops (predominantly diffuse but locally concentrated through swallow holes), while discharge takes place through springs at the southern border of the aquifer. There are three perennial outlets (Huertos, 560 m a.s.l.; Charco, 589 m a.s.l.; and La Zúa, 603 m a.s.l.) that are located in the tectonic contact between the Triassic dolostones and the metamorphic rocks of the IZ. There is also a temporary discharge area (overflow springs, 643 - 664 m a.s.l.) at the southern edge of the EZ, just North of the major tectonic contact between the IZ and the EZ (where low permeable Flysch clays are imbricated). In low water conditions, the water table is accessible through a shaft with a vertical development of 40 m at the overflow point.

3. METHODS

From October 2014 to December 2016 water temperature and electrical conductivity (EC) were recorded hourly in La Zúa (WTW™ Cond 315i), Charco, and Huertos springs (HOBO™ Onset U24-001), as well as in the shaft of the overflow springs (OTT™ EcoLog-800). Water level variations were registered in La Zúa (Odyssey™ Capacitance

Water Level) and the shaft (OTT™ EcoLog-800) and later transformed to a flow-rate data series. Additionally, single flow measurements were made at all the outlets, and samples for hydrochemical analysis were collected with a weekly to daily periodicity (depending on the hydroclimatic conditions).

Samples for major ion chemistry analysis were taken in 125 ml amber glass bottles, while 1L PET bottles were used for ^{3}H analysis. For noble gas determination, spring water was conducted through a transparent tube and collected in duplicate clamped-off copper cylinders, using a 12v submersible pump, following the procedure described by Sültenfuss et al. (2011). For CFC and SF_6 analysis, samples were collected in 500 ml double-opening steel bottles, as explained by Jaunat et al. (2012). To avoid CFC induced by the tubing material, a Viton hose was used to bring the water from the spring to the bottles. Suction was created using a peristaltic pump with a transparent tubing-outlet, which permitted the detection of bubbles that would indicate induced degassing. The steel bottles and the copper tubes were shaken after sealing, so that a lack of noise would make it possible to discard the involuntary formation of a headspace. Samples for groundwater dating were collected on five different dates, coinciding with diverse hydrodynamic situations: low, intermediate and high water conditions (LW, IW, and HW in Fig. 3).

Major chemical components were determined in the Laboratory of the Centre of Hydrogeology of the University of Malaga (CEHIUMA). Alkalinity was analyzed by volumetric titration with 0.02N H_2SO_4 to pH 4.45. Major ions (Ca^{2+}, Mg^{2+}, Na^{+}, K^{+}, Cl^{-}, SO_4^{2-}) were determined by ionic chromatography (METROHM Compact 930 IC flex for cations and Compact 881 IC Pro for anions). Determination of ^{3}H, He isotopes, Ne, CFC,

and SF_6 was carried out in the Department of Oceanography of the Institute of Environmental Physics, University of Bremen. He isotopes, Ne, and ^3H were determined at the mass spectrometric facility described by Sültenfuss, Roether, and Rhein (2009). As ^3H analysis followed the ^3He–ingrowth method (Clarke, Jenkins, & Top, 1976), water samples of 0.5 kg were degassed and stored in gas-free glass bulbs for production and accumulation of ^3He, the decay product of ^3H. After 4-6 months of storing, the ^3He produced was determined by means of the mass spectrometric system. Meanwhile, CFC and SF_6 concentrations were determined using a micro electron capture detector (micro-ECD) mounted on a gas chromatograph (Agilent GC6890N) with a capillary column, as explained by Bulsiewicz, Rose, Klatt, Putzka, and Roether (1998). The CFC data were calibrated according to the SIO scale 2005 (Bullister & Tanhua, 2010).

Noble gas concentrations are expressed in ccSTP/kg of H_2O —ccSTP being cubic centimeters at standard temperature and pressure. The specific radioactive activity of ^3H is expressed as Tritium Units (TU = 0.119 Bq/kg of H_2O). The CFC and SF_6 concentrations (pmol/kg of H_2O) were converted to an atmospheric mixing ratio (pptv) according to the recharge conditions: average recharge altitude of 1,150 m a.s.l., mean temperature of 8 ºC during rainy months (October to May), and no salinity. These conditions assume that recharge water rapidly reaches the saturated zone, which is consistant with dye tracer experiments at the site (De la Torre, 2020). Thus, no significant variations in water temperature should be expected, although a deep water table might exist in recharge areas.

The potential contribution of excess air was quantified as proposed by Aeschbach-Hertig, Peeters, Beyerle, and Kipfer (1999), based on the mean ΔNe values at each sample point. ΔNe is the ratio between the concentration of Ne in the sample and its theoretical content at recharge conditions minus 1, expressed as a percentage. An excess of up to 4% could be expected for this parameter, providing that the gases are equilibrated in the saturated zone, which could be some 500 m below the average recharge area, given the altitude of the springs.

The groundwater age of the sample fraction containing ^{3}H (recharged after 1953), was calculated using the $^{3}H/^{3}He$ method (Torgersen, Clarke, & Jenkins, 1978). The apparent piston flow $^{3}H/^{3}He$ age (τ) is given by:

$$\tau = \frac{1}{\lambda} \cdot ln\left(1 + \frac{^{3}He_{trit}}{^{3}He}\right) \qquad \text{(Equation 1)}$$

where λ is the ^{3}H decay constant, of 0.05626 yr^{-1} (ln(2)/12.32 yr; Lucas and Unterweger, 2000), and $^{3}He_{trit}$ (tritiogenic ^{3}He) is the concentration of that isotope in the sample derived from ^{3}H decay. Its separation from other ^{3}He sources in groundwater (equilibrium, excess-air, radiogenic) is possible using ^{4}He and Ne data (e.g. Cook & Herczeg, 2000; Sültenfuss et al., 2011). The CFC and SF_6 ages were determined by comparing their concentration in the sample and their mixing ratio in the Northern Hemisphere atmosphere (USGS, 2018). The ^{3}H input function used in modeling tasks was generated from correlation of the ^{3}H in precipitation recorded by the GNIP (Global Network of Isotopes in Precipitation) station closest to the pilot site (Morón, 55 km to the north) and the data series of the GNIP Vienna station (IAEA/WMO, 2018). The resulting

function was scaled to 2016; that is, it was converted to current concentration using the radioactive decay law and the ^{3}H decay constant. The difference with respect to the original and the decayed ^{3}H input functions gives rise to a $^{3}He_{trit}$ input function.

To interpret the groundwater age distributions of each sample, different models were created based on the concentration of ^{3}H, $^{3}He_{trit}$, $^{4}He_{rad}$ (radiogenic ^{4}He) and CFC-12 in samples taken during the same hydrodynamic conditions: high water or intermediate water (Table 2). TracerLPM software (Jurgens, Böhlke, Eberts, & Survey, 2012) was used to develop Lumped Parameter Models or LPMs (Maloszewski & Zuber, 1982). This kind of model uses a convolution integral to sum up all the tracer concentrations (C_i) at each possible time (t'). It incorporates a weight function $g(t-t')$ to determine the importance of each age in the total groundwater age at the sampling time (t) and a decay term for radioactive tracers based on the decay constant (λ):

$$C_s(t) = \int_{-\infty}^{t} C_i(t') \cdot g(t-t') \cdot e^{-\lambda(t-t')} dt' \qquad \text{(Equation 2)}$$

Additionally, Shape-Free models were created (Visser, Broers, Purtschert, Sültenfuß, & de Jonge, 2013). This approach is a simplification of equation 2, but instead of using a weight function, it describes the groundwater age distribution of the sample as a histogram of n bins having a uniform age. The number of bins is constrained by the number of tracers considered (n - *1*). The tracer concentration measured in the sample (C_s) is the sum of the products of the mean tracer concentration in each bin (C_i) and the fraction they represent in the whole groundwater sample (F_i):

$$C_s(t) = \sum_{i=1}^{n} F_i C_i(t') \qquad \text{(Equation 3)}$$

Two Shape-Free Models (SFMs) were used to describe the groundwater age distribution of each sample: 5-bin models were based on the four most reliable tracers (CFC-12, ^{3}H, $^{3}He_{trit}$, and $^{4}He_{rad}$) and 4-bin models were derived from the three young groundwater tracers. The latter model does not include ^{4}He data because its accumulation rate is uncertain. In both cases, the bins are equidistant except for the oldest one, which represents a sample fraction without recent age tracers (i.e., ^{3}H, $^{3}He_{trit}$, and CFC). The characteristics of each bin are shown in Table 3. The SFMs were developed using SOLVER Add-In in Excel. Each bin fraction was calculated adopting as constraints the piston-flow concentrations in the sample of the selected tracers.

4. RESULTS

4.1. Hydrodynamics and hydrochemistry

During the research period, the mean flow rates of the perennial outlets (IZ) varied from 23.4 l/s (Charco spring) to 208 l/s (La Zúa spring), with respective coefficients of variation of 15.1% and 16.1% (Table 1). These springs show buffered and delayed hydrodynamic responses to recharge events, reaching their flow peaks in several weeks or even months (Fig. 3). The discharge rate in the overflow area during periods of activity has an average value of 2.3 m^3/s, though it can reach 21.4 m^3/s. The water level variations in the shaft of the overflow area show a marked karst behavior, with quick rises in response to rainfall, as well as sudden drops (Fig. 3).

The mean contents of Ca^{2+}, Mg^{2+}, and SO_4^{2-} in the overflow springs are respectively 65.4 mg/l, 5.1 mg/l, and 8.3 mg/l, while alkalinity is 203.5 mg/l (Table 1). The

mineralization of groundwater greatly increases towards lower altitudes in the IZ (Fig. 3) —particularly Ca^{2+}, Mg^{2+}, and SO_4^{2-}, which respectively reach average values up to 437.3 mg/l, 87 mg/l, and 1201.1 mg/l in Huertos spring (Table 1). Such changes in the hydrochemistry of groundwater make EC rise at lower altitudes (Fig. 3), from mean values of 352 µS/cm in the overflow outlets, to averages between 1565 µS/cm and 1875 µS/cm in the IZ (Tab. 1). Likewise, the mean temperature value of the groundwater drained through the overflow area is 14.9 ºC, while it is between 15.7 ºC and 16.7 ºC in the IZ springs.

The variability of the physicochemical parameters monitored in the overflow springs is much higher than in the outlets of the IZ, as shown by their coefficients of variation (Table 1). While the water temperature and the EC values registered in the overflow area change substantially and rapidly, the variations of these two parameters are smoother and delayed in the perennial springs of the IZ. Moreover, the concentration of Mg^{2+} is found to be more stable than the contents of Ca^{2+} and SO_4^{2-}; yet Mg^{2+} and SO_4^{2-} are more stable in the overflow area than in the perennial outlets (Fig. 3). The temporal hydrochemical evolution of the springs therefore reflects two clearly distinct patterns depending on the geological location of the springs in the aquifer.

4.2. Environmental tracers

The ΔNe values of the samples range from 27.0% to 39.4%, indicating some air excess in the samples (Table 2). The ΔNe of the duplicate differs 5% at most, meaning the excess is not due to inadequate sampling, but rather to the dissolution of air bubbles trapped in the soil zone or the aquifer during recharge (Aeschbach-Hertig et al., 1999;

Mayer et al., 2014). The ΔNe values allow the fraction of gases in the sample from excess air to be estimated, including ^{4}He isotopes (Aeschbach-Hertig et al., 1999). Non-atmospheric ^{4}He is of underground radiogenic origin ($^{4}He_{rad}$) and produced by alpha decay of the U and Th decay series. The remaining ^{4}He (excluding excess air and radiogenic) comes from the atmosphere (solubility equilibrium). Assuming that the liberation rate of the $^{4}He_{rad}$ to groundwater is constant and homogeneous, its concentration would be proportional to groundwater travel time (Solomon, 2000).

The concentrations of $^{4}He_{rad}$ in the samples range from $1.3 \cdot 10^{-5}$ to $2.6 \cdot 10^{-5}$ ccSTP/kg (Table 2). A rise in the content of $^{4}He_{rad}$ is observed from La Zúa to Huertos spring, from higher to lower altitudes (Fig. 4), which would also indicate an increase of the mean residence time. The $^{4}He_{rad}$ accumulation rates reported in the literature vary two orders of magnitude, from $2.0 \cdot 10^{-8}$ ccSTP$\cdot$kg$^{-1}\cdot$yr^{-1} (Lehmann et al., 2003) to $1.9 \cdot 10^{-6}$ ccSTP$\cdot$kg$^{-1}\cdot$yr^{-1} (Beyerle et al., 1999), so it is not possible to estimate a reliable $^{4}He_{rad}$ age using these values. Nevertheless, assuming the fastest accumulation rate, of $1.9 \cdot 10^{-6}$ ccSTP$\cdot$kg$^{-1}\cdot$yr^{-1}, the observed data would require —at least— mean residence times of around a decade. The slowest accumulation rates would lead to residence times up to two orders of magnitude higher.

All the samples contain ^{3}H, between 1.65 and 2.46 TU (Table 2). The ^{3}H activity in precipitation registered in SW Spain by the GNIP from 1980 (IAEA/WMO, 2018), scaled to 2016, lies in the same range (De la Torre, 2020). Therefore, the concentrations observed in the samples could correspond to piston flow ages in that period; in other words, an unmixed groundwater sample with such ^{3}H content would have been recharged

within that interval. The $^{3}H/^{3}He$ dating results give infiltration ages between 33 and 40 years (Table 2), fairly consistent with the mentioned period. Small rises in the piston-flow ages deduced from $^{3}H/^{3}He$ (~2 years) suggest ^{3}H activit duplicating the observed data. Thus, although the presence of tritium-free groundwater in the sample could reduce ^{3}H activity without affecting the $^{3}H/^{3}He$ ratio, binary mixing of a piston-flow distribution and an old component cannot be completely discarded in this case.

The measured CFC-12 values vary from 0.98 to 1.58 pmol/kg, which correspond to atmospheric mixing ratios of 184 and 295 pptv (Table 2) at the infiltration conditions of temperature and pressure (see section 3). Note that the effect of using different ΔNe within the observed range in each spring would affect the CFC-12 mixing ratios of less than 5 pptv, having no practical effect on dating estimations. The results would indicate piston flow ages from 36 to 43 years, which are slightly older than the $^{3}H/^{3}He$ ages (Table 2). Such differences could be caused by small changes in temperature under the recharge conditions (Gil-Márquez, Sültenfuß, Andreo & Mudarra, 2020). They might also be related to a diluted CFC-12 concentration owing to the presence of an old component with a lower tracer content, or free of it. Although dilution would cause a bias toward older CFC-12 ages, it would not modify the $^{3}H/^{3}He$. Some CFC-12 diminishing could also be produced through sorption or microbial degradation, but it is unlikely, since CFC-12 sorption is generally negligible (Cook & Solomon, 1997) and its degradation requires anoxic conditions (IAEA, 2006), which is not the case of the springs of the IZ (mean dissolved oxygen = 4.5 mg/l).

CFC-11 values are between 1.27 and 2.28 pmol/kg, equivalent to 62 and 111 pptv, respectively (Table 2). Such values are much lower than the ones expected from CFC-12 data and are not explained by mixing models. As no contamination sources exist in the recharge area, CFC-11 concentrations in the groundwater would have been diminished by sorption or another physical or biochemical process. Accordingly, microbial degradation affects the CFC-11 more than the CFC-12 contents (IAEA, 2006). To the contrary, the contents of SF_6 in the sample (0.17 - 0.22 pmol/kg) are related to extremely high SF_6 mixing ratios, over 450 pptv (Table 2). Such results are more than one order of magnitude higher than the current atmospheric mixing ratios (approximately 10 pptv); without a nearby source of pollution, they can be explained only by terrigenic production. The predominant dolostone formations in the aquifer may be the natural source of SF_6 (Busenberg and Plummer, 2000). Neither CFC-11 nor SF_6 are reliable references for the mixing models.

4.3. Groundwater mixing and age distribution models

To find a model that properly describes the groundwater age distribution of our samples, each possible type of Lumped Parameter Model (LPM) was checked: Piston Flow Model (PFM), Exponential Model (EM), Partial Exponential Model (PEM), Exponential Piston Model (EPM), and Dispersion Model (DM) (e.g. Jurgens et al., 2012; Suckow, 2014). In general terms, none of them show a good fit to the sample concentrations. A binary mixing process could explain the tracer concentrations, however.

In Figure 5, the spring samples are plotted in three tracer-tracer graphs together with their evolution according to the PFM and the DM (dispersion parameter = 0.05). The samples plot in areas between two theoretical mixing lines, drawn from two different modern groundwater components, of 0 and 40 years, with an old component (free of ^{3}H and CFC-12). Thus the tracer concentration measured in the sample could be explained by a Binary Mixing Model (BMM). In view of this possibility, two BMMs were created for each sample, one simplified proxy combining two PFMs, the other one integrating two DMs, a type of LPM applicable to diverse hydrogeological settings (Jurgens et al., 2012). The dispersion parameter of the DM that describes the young fraction of the BMM is 0.05, and its mean age ranges from 25 to 31 years, depending on the sample. The dispersion parameter in the old DM is 0.2, and the mean ages are 160 years for La Zúa and Charco springs, and 200 years for Huertos spring.

Different accumulation rates of $^{4}He_{rad}$ were checked to include it in the LPMs. The value was adjusted so that all the estimated old fractions of the BMM (DM-DM) could explain the $^{4}He_{rad}$ concentrations observed, assuming a constant accumulation rate within the aquifer. The best results were obtained with a value of $2 \cdot 10^{-7}$ STPcc$\cdot kg^{-1} \cdot yr^{-1}$. This rate gave an estimated $^{4}He_{rad}$ age for each sample (Tab. 2) between 66 years (La Zúa) and 131 years (Charco). Yet other values were used to define the old fraction of the LPM, as the $^{4}He_{rad}$ content in the sample would be diluted by the younger component. The $^{4}He_{rad}$ accumulation rate permitted inclusion of this tracer to create an SFM of 5 bins. As the concentration of this tracer in each bin is derived from another model (BMM DM-DM), the 4-bin SFM was also generated without $^{4}He_{rad}$.

Table 4 offers a summary of the most relevant data extracted from each model. Both types of LPMs suggest that the percentage of the old component (free of ^{3}H and CFC-12) is greater in Huertos spring, and its ratio is low in La Zúa. This pattern is furthermore observed in the results obtained when applying SFMs (Table 4). Hence the proportion of groundwater infiltrated before 1940 is greater at low altitudes.

The mean age of the groundwater samples could only be estimated by models including $^{4}He_{rad}$ data (BMM DM-DM and 5-bin SFM), as the other two models (BMM PFM-PFM and 4-bin SFM) were created based on ^{3}H and CFC-12, which afford no information about the age of the old fraction of samples. The mean age findings differ considerably depending on the model (Table 4): from 15 years of difference in La Zúa spring (54 and 69 years) to 35 years in Huertos spring (95 and 123 years). Nonetheless, in both cases the mean age of the samples increases from the highest altitude (La Zúa) to the lowest (Huertos). It is also noteworthy that all the mean ages indicate several decades of average transit time. Ages over 63 years point to a mean infiltration date before the anthropogenic liberation of ^{3}H (1953), whereas values over 76 would also be previous to the generation of CFC-12 (1940).

The groundwater age distribution of the samples was calculated by applying the LPMs and the SFMs (Fig. 6). All the models show that La Zúa spring accumulates a higher proportion of young water, while the groundwater age distributions of the samples from Charco and Huertos springs are progressively biased towards older ages. The two samples of Huertos and Charco springs have a similar distribution, regardless of the hydrodynamic conditions in which they were collected. The samples from La Zúa springs show some

differences (Fig. 6) —the sample taken in high water conditions (December 2016) accumulates a lesser proportion of young groundwater than the one collected in an intermediate water state (October 2014).

The median of the Groundwater Age distribution (heretofore GA50) can be easily identified in groundwater distribution plots, in the bin (for SFM) or age bracket (for LPM) in which the cumulative fraction reaches or exceeds 50% (Gil-Márquez et al., 2020). This parameter helps to rapidly assess whether the sample is formed mainly by recent or older groundwater, as opposed to the mean age, which sometimes leads to misinterpretation of mixed groundwater age data. The GA_{50} could be more than 80 years in all the spring according to the 5-bin SFM (Table 4 and Fig. 6), while the lowest values are obtained from the BMM DM-DM, with a GA_{50} of 30 years in La Zúa spring, 44 years in Charco, and 60 years in Huertos. The groundwater drained by the spring therefore accumulates a lesser modern fraction toward lower altitudes.

5. DISCUSSION

5.1. Coupling hydrochemistry and groundwater age distribution

Variations in dating environmental-tracer concentrations under different hydrodynamic conditions (Table 2) can provide information about the functioning of an aquifer. Here it was found that the $^{4}He_{rad}$ concentration rises from high water (HW) to low water (LW) conditions, meaning that in recession periods the mix of groundwater drained through the spring is older than in discharge rises. This interpretation is compatible with the increment of mineralization registered in dry periods (Fig. 3). The

only exception is that of La Zúa spring, where the highest $^{4}He_{rad}$ content was obtained in high water conditions (Table 2), attributed to a piston-flow effect during sampling (Fig. 3). As used in karst hydrogeology, this term describes increased mineralization and water temperature in a spring in response to recharge events, often owing to the mobilization of older groundwater from the saturated zone (e.g., Mudarra & Andreo, 2011). The decreased ^{3}H contents in low water conditions (Table 2) could likewise be produced by a higher proportion of old groundwater (tritium-free) being drained. The evolution of the ^{3}H input function and the seasonal fluctuations of this isotope in the atmosphere make it difficult to arrive at conclusions with just a few samples. Delbart et al. (2014) underlined that an exhaustive sampling routine would help determine the evolution of young-groundwater tracers (not only ^{3}H, but also CFC and SF_6), particularly during discharge rises. The present work demonstrates the potential of an old-groundwater tracer ($^{4}He_{rad}$) when analyzing the natural response of karst springs.

In Figure 7 and Table 5 certain physicochemical and chemical parameters are compared to groundwater dating data derived from the LPMs and the SFMs. Electrical conductivity (EC) is seen to be positively related to the proportion of old groundwater (free of ^{3}H and CFC-12) and the mean and median age of the samples (Figs. 7A & B), the obtained p-values being generally lower than 0.05 (Table 5). The ascent of EC is also related to a decrease in the spring height (Fig. 3). Taken together, this indicates that the groundwater drained by the springs at lower altitudes had a longer residence time within the aquifer, thus a greater amount of dissolved solutes (i.e., higher EC).

A similar relationship is established between the groundwater dating parameters and the temperature values measured in the spring water (Figs. 7C & D), which are slightly higher (1-2 ºC) than the mean annual temperature of the area (De la Torre, Mudarra, & Andreo, 2020), although the correlations are not always statistically significant within a 95% confindence limit (p-value > 0.05; Table 5). Besides, the variability of the water temperature of the springs located in the IZ is low (<1%), contrary to the variability of the flow rate and most of the chemical parameters (Table 1), and also to the groundwater temperature in the overflow area. All this information suggests that groundwater may flow within deep areas of the system. But the lack of thermalism *stricto sensu* would indicate a slow ascent of groundwater flows toward the discharge points, progressively reaching temperature values near the equilibrium with the atmosphere.

The water mineralization of the springs in the IZ is mainly related to dissolved SO_4^{2-}, Ca^{2+}, and Mg^{2+} contents (Table 1). The presence of SO_4^{2-} and Ca^{2+} in the groundwater of Jarastepar aquifer makes possible the dedolomitization of Triassic dolostone rocks of the EZ. This geochemical process entails multi-mineral phases and consists of the transformation of dolomite crystals into calcite (Appelo & Postma, 2005; Wigley, 1973), resulting in a greater amount of dissolved Mg^{2+} in groundwater than could be explained by dolomite dissolution alone. While the concentration of Mg^{2+} in groundwater shows a marked increase towards lower altitudes, the rise of Ca^{2+} is less steep (Fig. 3). Besides, the molar relation between Mg^{2+} and Ca^{2+} (rMg/Ca) presents a positive and well-defined relationship with the percentage of old groundwater in the samples and their mean and median ages (Fig. 7E & F). Therefore, there was an enrichment of Mg^{2+} with respect to

Ca^{2+} as groundwater became older; hence the lower the spring´s altitude, the more hydrogeochemically evolved the groundwater it drains, given longer water-rock interactions. This process has been described in other carbonate systems worlwide (Carucci, Petitta, & Aravena, 2012; McMahon, Böhlke, & Christenson, 2004; Moral, Cruz-Sanjulián, & Olías, 2008; Plummer et al., 1990). The good degree of correlation between the dating parameters obtained from the models and the rMg/Ca (p-value < 0.05; Tab. 5) indicates that the groundwater of Jarastepar aquifer is mainly stored in dolomite-bearing formations, which form the permeable layers in the IZ and the deepest part of the aquifer in the EZ (Figs. 1 & 2).

Dissolution of the evaporite rocks from the EZ is the main source of SO_4^{2-} and Ca^{2+} in the groundwater of the aquifer, according to the strong stoichiometric relationship of both ions and to the isotope signature of $\delta^{34}S_{SO4}$ and $\delta^{18}O_{SO4}$ (De la Torre et al., 2020). The SO_4^{2-} concentration in the samples is positively related to the presence of old groundwater and the mean and median ages (Figs. 7G & H). However, the degree of correlation is lower than that found for EC and rMg/Ca (Table 5). This could indicate that gypsum dissolution does not occur during all the groundwater transit time, contrary to de-dolomitization. Thus, groundwater would dissolve gypsum within the EZ substratum, which would enhance the gain in Mg^{2+} through de-dolomitization, although it cannot be discarded that some of the Mg^{2+} present in the groundwater comes from the dissolution of evaporite rocks (Hamill & Bell, 1986; Chenini, Farhat & Ben Mammou, 2010.). After groundwater enters the IZ, the dissolution of gypsum ends (since there are no evaporites

in the IZ), but the SO_4^{2-} concentration is still high, allowing de-dolomitization to last longer while groundwater flows within the Triassic dolostone formation.

The low degree of correlation between groundwater age parameters and SO_4^{2-} (Table 5) is partly due to the large variations in the concentration of this ion in the spring waters, particularly in La Zúa (Figs. 7G & H). The higher outflow rate of La Zúa spring and its greater hydrodynamic response (Table 1, Fig. 3) signal a better hydrogeological connection with the External Zone. That would explain the higher variability of SO_4^{2-}, whose source is in the External Zone, as well as the changes in the groundwater age distribution that are observed in every model made from the samples of the spring (Table 4; Fig. 7). Despite the fact that the groundwater age distributions of Huertos and Charco springs do not evidence much variations, it cannot be discarded that a higher number of analyses of dating environmental tracers could show otherwise.

5.2. Implications of the geological setting on the groundwater residence time

In all the SFMs, a significant accumulation of groundwater from 20 to 60 years of age is observed, while the fraction does not change in the immediately following bin (Fig. 6). Therefore, the remaining groundwater fraction is attributable to the old bin (free of ^3H and CFC-12). The groundwater age distributions obtained from the SFMs —which do not require any previous assumption of the hydrogeological functioning of the system— agree with the binary mixing LPMs proposed. They confirm that the drainage of Jarastepar aquifer is explained by two main flow components. One is formed by groundwater infiltrated during the last few decades, while the other has a much longer

mean residence time of around 200 years. The groundwater age distribution of the springs of the IZ contrast with the high flow velocities determined in the EZ of the aquifer (overflow area in Figure 1) using dye tracing tests, which reached 600 m/h (De la Torre, 2020).

Substantial development of the conduit network in the EZ confers it a large drainage capacity, allowing for fast arrival of recently infiltrated water towards the overflow area. There, temporary outlets drain the aquifer only when the water coming from recharge exceeds the transfer capacity between the IZ and the EZ, given the hydraulic hetereogeneity of the media. The chemical signature of the groundwater drained through the overflow area and the dye tracing evidence that this water is mostly related to the recharge events that activate temporary outlets, and it has a mean residence time of 54-64 hours (De la Torre et al., 2020). This behavior is typical in karst areas, where the mean residence time of groundwater is between tens of hours to several months, as inferred from natural and artificial responses of the springs (Barberá et al., 2018; Birk, Liedl, & Sauter, 2004; Lauber & Goldscheider, 2014; Perrin, Jeannin, & Zwahlen, 2003; Shah et al., 2017). However, these age estimations reflect only the fastest flowpaths throughout the conducts, not the slower flows through narrow fractures and the matrix, which must be estimated based on environmental tracers (Worthington & Gunn, 2009). It is therefore necessary to understand the intrinsic characteristics of the media when interpreting groundwater dating data.

The geological complexity of the Jarastepar aquifer —and particularly the existence of a major tectonic contact with imbrication of impervious materials (Flysch), together

with the great thickness of the semi-confined Jurassic and Triassic calcareous formations— confers the springs placed in the IZ of the aquifer lagged and buffer responses to precipitation events (Fig. 3). This may be considered typical behavior for springs draining carbonate aquifers with dominated fissured or diffuse flow functioning (Jeannin, Groves, & Häuselmann, 2007; Mudarra & Andreo, 2011; Perrin et al., 2003). Yet the mean ages estimated in this case nearly reach the century (Table 4) instead of a few years or decades, as in other small alpine karst aquifers (Althaus et al., 2009; Lauber & Goldscheider, 2014). In addition, the models point to the existence of an old flow component with a mean residence times of around 200 years (Table 4). Such binary mixing with centennial groundwater is normally observed in large carbonate aquifers, often partially confined, in which a long-tailed age distribution is defined (Jiang et al., 2019; Toth & Katz, 2006; Yager et al., 2010; Zang et al., 2015). The Jarastepar aquifer is far from that definition —its outcropping surface is 56 km^2, mostly corresponding to the unconfined EZ, and can be rapidly drained through the overflow springs. The distance from the tectonic suture to the perennial outlets is short, particularly to the southwest, where the overflow area is 600 m away from Huertos spring (Fig. 1). Assuming a straight-forward flow connecting both points, the groundwater would have a velocity of 6 m/year, as the mean residence time of the groundwater drained by Huertos spring is estimated at nearly 100 years (Table 4), and the groundwater drained through the overflow springs is infiltrated just a few hours before. Such flow velocities do not seem reasonable in karst formations.

Based on geological observations and hydrogeological methods (hydrochemistry, hydrodynamics, stable isotopes), De la Torre et al. (2020) proposed a hydrogeological conceptual model of the aquifer that helps to understand the presence of old groundwater. The existence of an imbricated layer (discontinuous because of tectonics) between the EZ and the IZ, formed by Flysch-type clays and sandstones and Cretaceous-Tertiary marls and marly limestones, slows down the transference of groundwater from the Jurassic carbonate formation (EZ) to the Triassic dolomites (IZ). This groundwater comes from the saturated zone and is older than that drained through the overflow springs (Fig. 8). Additionally, the flow deceleration produced by the low permeability formations would mean a longer residence time of groundwater within the media. Altogether, such a scenario would explain the existence of young groundwater components in the permanent springs with mean transit times of few decades (Table 4 and Fig. 6).

The presence of an old groundwater flow component is attributable to the combined thickness of the Jurassic and the Triassic carbonate formations, up to 1000 m. Both units are partially confined below the metamorphic formations of the IZ and their southward extension is unknown. Furthermore, the karstification degree and the permeability of the dolostones of the IZ are lower than in the EZ. In any case, groundwater can only leave the system through the perennial springs; thus, after it traverses a long flowpath to deep areas of the aquifer, the tectonic contact with the low permeable rocks forces the ascent of the groundwater flow towards the outlets (Fig. 8). In view of the low water temperature (Table 1), upwelling through the Triassic dolomite formation must occur slowly, allowing a greater transference of Mg^{2+} to the groundwater and a temperature re-equilibrium. This

explains why the correlation of groundwater age parameters with rMg/Ca is high, while it is lower with SO_4^{2-} (Table 5).

These findings not only demonstrate the existence of centennial groundwater in a realtively small alpine karst aquifer, but they also show how the features of the geological framework can condition flow dynamics and residence time. There is little evidence of centennial groundwater in this type of system, except for some karst springs in the Austrian Alps that drain deep reservoirs connected to major faults (Han et al., 2007; Hilberg & Schneider, 2011). The fact that the groundwater age in alpine karst can be this old has major implications for hydrogeological management, and regarding its intrinsic vulnerability to pollution. Therefore, contrary to what might be expected, the complementary use of environmental dating tracers and hydrochemistry in complex carbonate formations can prove useful for the management of groundwater resources, particularly if the structure of the aquifer is complex.

6. CONCLUSIONS

In this research, conventional hydrogeological methods used in karst aquifer studies (hydrochemistry, hydrodynamics, and water temperature) were jointly applied with groundwater dating tools (^3H, ^3He, ^4He, CFC-12, CFC-11, and SF_6) to explain the functioning of a complex and relatively small alpine karst aquifer. Based on the environmental-tracer concentrations, both Lumped Parameter Models and Free-Shape Models were created to determine the groundwater-age distribution of the spring water under different hydrodynamic conditions. All this made it possible to identify two main flow components in the mix drained through the springs, and to assess their groundwater

age distribution. Such binary mixing is coherent with karst systems in which conduit flow and diffuse flow coexist. Here, however, the mean ages of the springs are several decades, and the old component could be some 200 years old. Because these transit times are long for a relatively small alpine karst area, they can only be explained by a complex geological setting, including a major tectonic contact that involves imbricated material of low permeability and a thick semiconfined saturated zone.

The hydrochemical characteristics of the springs —and especially the rise in mineralization and rMg/Ca values towards lower altitudes— are compatible with long residence times. Moreover, the natural responses registered in the spring waters, including variations in the contents of radiogenic ^{4}He, are coherent with the binary mixing described. Even though the number of samples analyzed was limited in this case, studying the evolution of environmental tracer concentrations in the water of karst springs can be seen as an aid for hydrogeological understanding.

The results presented here demonstrate the applicability of environmental dating tracers in karst areas located in alpine mountains, and their usefulness for interpreting hydrogeological functioning when combined with hydrochemical data and natural response analysis. This methodological approach is potentially useful for the study of other alpine karst aquifers having complex geology. Determining the age distribution of groundwater drained through karst springs is crucial for the assessment of pollution vulnerability and the definition of safeguard zones for groundwater protection.

7. REFERENCES

Aeschbach-Hertig, Peeters, F., Beyerle, U., & Kipfer, R. (1999). Interpretation of dissolved

atmospheric noble gases in natural waters. *Water Resources Research*, *35*(9), 2779–2792.

Akesson, M., Suckow, A., Visser, A., Sültenfuss, J., Laier, T., Purtschert, R., & Sparrenbom, C. J. (2015). Constraining age distributions of groundwater from public supply wells in diverse hydrogeological settings in Scania, Sweden. *Journal of Hydrology*, *528*, 217–229. https://doi.org/10.1016/j.jhydrol.2015.06.022

Althaus, R., Klump, S., Onnis, A., Kipfer, R., Purtschert, R., Stauffer, F., & Kinzelbach, W. (2009). Noble gas tracers for characterisation of flow dynamics and origin of groundwater: A case study in Switzerland. *Journal of Hydrology*, *370*(1–4), 64–72. https://doi.org/10.1016/j.jhydrol.2009.02.053

Appelo, C. A. J., & Postma, D. (2005). *Geochemistry, Groundwater and Pollution* (2nd ed.). Amsterdam: A.A. Balkema publishers.

Bailly-Comte, V., Martin, J. B., & Screaton, E. J. (2011). Time variant cross correlation to assess residence time of water and implication for hydraulics of a sink-rise karst system. *Water Resources Research*, *47*(5), 1–16. https://doi.org/10.1029/2010WR009613

Ballesteros, D., Jiménez-Sánchez, M., Giralt, S., García-Sansegundo, J., & Meléndez-Asensio, M. (2015). A multi-method approach for speleogenetic research on alpine karst caves. Torca La Texa shaft, Picos de Europa (Spain). *Geomorphology*, *247*, 35–54. https://doi.org/10.1016/j.geomorph.2015.02.026

Barberá, J. A. A., Mudarra, M., Andreo, B., & De la Torre, B. (2018). Regional-scale analysis of karst underground flow deduced from tracing experiments: examples from carbonate aquifers in Malaga province, southern Spain. *Hydrogeology Journal*, *26*(1), 23–40. https://doi.org/10.1007/s10040-017-1638-5

Barberá, J. A. A., Mudarra, M., Andreo, B., De la Torre, B., & la Torre, B. (2018). Regional-scale

analysis of karst underground flow deduced from tracing experiments: examples from carbonate aquifers in Malaga province, southern Spain. *Hydrogeology Journal*, *26*(1), 23–40. https://doi.org/10.1007/s10040-017-1638-5

Beyerle, U., Aeschbach-Hertig, W., Hofer, M., Imboden, D. M., Baur, H., & Kipfer, R. (1999). Infiltration of river water to a shallow aquifer investigated with H-3/He-3, noble gases and CFCs. *Journal of Hydrology*, *220*(3–4), 169–185.

Birk, S., Liedl, R., & Sauter, M. (2004). Identification of localised recharge and conduit flow by combined analysis of hydraulic and physico-chemical spring responses (Urenbrunnen, SW-Germany). *Journal of Hydrology*, *286*(1–4), 179–193. https://doi.org/10.1016/j.jhydrol.2003.09.007

Bullister, J. L., & Tanhua, T. (2010). Sampling and Measurement of Chlorofluorocarbons and Sulfur. In E. . Hood, C. L. Sabne, & B. . Sloyan (Eds.), *The GO-SHIP repeat hydrography manual: a collection of expert reports and guidelines*. IOCCP Report Number 14, ICPO Public ation Series Number 134.

Bulsiewicz, K., Rose, H., Klatt, O., Putzka, A., & Roether, W. (1998). A capillary-column chromatographic system for efficient chlorofluorocarbon measurement in ocean waters. *Journal of Geophysical Research*, *103*(C8), 15959–15970. https://doi.org/10.1029/98JC00140

Cartwright, I., Weaver, T. R., Stone, D., & Reid, M. (2007). Constraining modern and historical recharge from bore hydrographs, 3H, 14C, and chloride concentrations: Applications to dual-porosity aquifers in dryland salinity areas, Murray Basin, Australia. *Journal of Hydrology*, *332*(1–2), 69–92. https://doi.org/10.1016/j.jhydrol.2006.06.034

Carucci, V., Petitta, M., & Aravena, R. (2012). Interaction between shallow and deep aquifers in

the Tivoli Plain (Central Italy) enhanced by groundwater extraction: A multi-isotope approach and geochemical modeling. *Applied Geochemistry*, *27*(1), 266–280. https://doi.org/10.1016/j.apgeochem.2011.11.007

Castro, M. C., Stute, M., Schlosser, P., Clara, M., Stute, M., & Schlosser, P. (2000). Comparison of 4He ages and 14C ages in simple aquifer systems: implications for groundwater flow and chronologies. *Applied Geochemistry*, *15*, 1137–1167.

Clarke, W. B., Jenkins, W. J., & Top, Z. (1976). Determination of tritium by mass spectrometric measurement of 3He. *International Journal of Applied Radiation and Isotopes*, *27*(9), 515–522.

Cook, P. G., & Solomon, D. K. (1997). Recent advances in dating young groundwater: Chlorofluorocarbons, 3H/3He and 85Kr. *Journal of Hydrology*, *191*(1–4), 245–265. https://doi.org/10.1016/S0022-1694(96)03051-X

Cook, P., Solomon, D. K., Sanford, W. E., Busenberg, E., & Plummer, L. N. (1996). Inferring shallow groundwater flow in saprolite and fractured rock using environmental tracers. *Water Resources Research*, *32*(6), 1501–1509.

Cook, P.G., Love, A. J., Robinson, N. I., & Simmons, C. T. (2005). Groundwater ages in fractured rock aquifers. *Journal of Hydrology*, *308*(1–4), 284–301. https://doi.org/10.1016/j.jhydrol.2004.11.005

Cook, P G, & Bohlke, J. K. (2000). Determining timescales for groundwater flow and solute tranport. In P.G. Cook & A. L. Herczeg (Eds.), *Environmental tracers in subsurface hydrology* (pp. 1–30). New York: Springer sciences+Business Media.

Cook, Peter G., & Herczeg, A. L. (2000). *Environmental Tracers in Subsurface Hydrology*. (Peter G. Cook & A. L. Herczeg, Eds.), *Book*. New York: Springer Science/Business Media.

https://doi.org/10.1017/CBO9781107415324.004

Corcho Alvarado, J. A., Purtschert, R., Barbecot, F., Chabault, C., Rueedi, J., Schneider, V., … Loosli, H. H. (2007). Constraining the age distribution of highly mixed groundwater using ^{39}Ar: A multiple environmental tracer (^{3}H/^{3}He, ^{85}Kr, ^{39}Ar, and ^{14}C) study in the semiconfined Fontainebleau Sands Aquifer. *Water Resources Research*, *43*(3), 1–16. https://doi.org/10.1029/2006WR005096

De la Torre, B., Mudarra, M., & Andreo, B. (2020). Investigating karst aquifers in tectonically complex alpine areas coupling geological and hydrogeological methods. *Journal of Hydrology X*, *6*(November 2019), 100047. https://doi.org/10.1016/j.hydroa.2019.100047

Delbart, C., Barbecot, F., Valdes, D., Tognelli, A., Fourre, E., Purtschert, R., … Jean-Baptiste, P. (2014). Investigation of young water inflow in karst aquifers using SF_6-CFC-^{3}H/He-^{85}Kr-^{39}Ar and stable isotope components. *Applied Geochemistry*, *50*, 164–176. https://doi.org/10.1016/j.apgeochem.2014.01.011

Ebrahimi, B., Pasandi, M., & Ahmadipour, M. R. (2007). Hydrodynamic behaviour of karstic aquifers in Boroujerd, western Iran. *Hydrological Sciences Journal*, *52*(1), 192–205. https://doi.org/10.1623/hysj.52.1.192

Elliot, T. (2014). Environmental tracers. *Water (Switzerland)*, *6*(11), 3264–3269. https://doi.org/10.3390/w6113264

Field, M. S. S. (1999). *A Lexicon of Cave and Karst Terminology with Special Reference to Environmental Karst Hydrology*. (U. E. P. Agency, Ed.), *Environmental Protection*. Washington, D.C.: US Environmental Protection Agency. Retrieved from http://www.vnovak.hr/speleo/znanost/terminologija/glossary.pdf

Ford, D. C. (1983). Alpine karst systems at crowsnest pass, Alberta-British Columbia, Canada.

Journal of Hydrology, *61*, 187–192.

Gardner, P. M., & Heilweil, V. M. (2014). A multiple-tracer approach to understanding regional groundwater flow in the Snake Valley area of the eastern Great Basin, USA. *Applied Geochemistry*, *45*, 33–49. https://doi.org/10.1016/j.apgeochem.2014.02.010

Gil-Márquez, J. M., Sültenfuß, J., Andreo, B., & Mudarra, M. (2020). Groundwater dating tools (3H, 3He, 4He, CFC-12, SF6) coupled with hydrochemistry to evaluate the hydrogeological functioning of complex evaporite-karst settings. *Journal of Hydrology*, *580*(May 2019), 124263. https://doi.org/10.1016/j.jhydrol.2019.124263

Goldscheider, N., & Drew, D. (2007). *Methods In Karst Hydrogeology*. London: Taylor & Francis.

Han, L., Hacker, P., & Gröning, M. (2007). Residence times and age distributions of spring waters at the Semmering catchment area, Eastern Austria, as inferred from tritium, CFCs and stable isotopes. *Isotopes in Environmental and Health Studies*, *43*(1), 31–50. https://doi.org/10.1080/10256010601154015

Hilberg, S., & Schneider, J. F. (2011). The Aquifer Characteristics of the Dolomite Formation a New Approach for Providing Drinking Water in the Northern Calcareous Alps Region in Germany and Austria. *Water Resources Management*, *25*(11), 2705–2729. https://doi.org/10.1007/s11269-011-9834-x

Hu, K., Chen, H., Nie, Y., & Wang, K. (2015). Seasonal recharge and mean residence times of soil and epikarst water in a small karst catchment of southwest China. *Scientific Reports*, *5*(May), 1–12. https://doi.org/10.1038/srep10215

IAEA/WMO. (2018). Global Network of Isotopes in Precipitation. The GNIP Database.

IAEA. (2006). *Use of Chlorofluorocarbons in Hydrology: a guidebook. International Atomic Energy Agency*. Vienna: International Atomic Energy Agency. Retrieved from http://scholar.google.com/scholar?hl=en&btnG=Search&q=intitle:Use+of+chlorofluorocarbons+in+hydrology#2

Jasechko, S. (2016). Partitioning young and old groundwater with geochemical tracers. *Chemical Geology*, *427*, 35–42. https://doi.org/10.1016/j.chemgeo.2016.02.012

Jasechko, S., Perrone, D., Befus, K. M., Bayani Cardenas, M., Ferguson, G., Gleeson, T., … Kirchner, J. W. (2017). Global aquifers dominated by fossil groundwaters but wells vulnerable to modern contamination. *Nature Geoscience*, (April), 1–6. https://doi.org/10.1038/ngeo2943

Jaunat, J., Huneau, F., Dupuy, A., Celle-Jeanton, H., Vergnaud-Ayraud, V., Aquilina, L., … Le Coustumer, P. (2012). Hydrochemical data and groundwater dating to infer differential flowpaths through weathered profiles of a fractured aquifer. *Applied Geochemistry*, *27*(10), 2053–2067. https://doi.org/10.1016/j.apgeochem.2012.06.009

Jeannin, P. Y., Groves, C., & Häuselmann, P. (2007). Speleological invesitgations. In N. Goldscheider & D. Drew (Eds.), *Methods in karst hydrogeology* (pp. 25–44). London: Taylor & Francis.

Jiang, G., Guo, F., & Tang, C. (2019). Groundwater systems in bare and covered karst aquifers: evidence from tracer tests, hydrochemistry, and groundwater ages. *Environmental Earth Sciences*, *78*(20), 1–14. https://doi.org/10.1007/s12665-019-8622-4

Jurgens, B. C., Böhlke, J. K., Eberts, S. M., & Survey, U. S. G. (2012). TracerLPM (Version 1): An Excel® workbook for interpreting groundwater age distributions from environmental tracer data. *Techniques and Methods*, (Version 1). Retrieved from

http://pubs.er.usgs.gov/publication/tm4F3

Katz, B. G., Chelette, A. R., & Pratt, T. R. (2004). Use of chemical and isotopic tracers to assess nitrate contamination and ground-water age, Woodville Karst Plain, USA. *Journal of Hydrology*, *289*(1–4), 36–61. https://doi.org/10.1016/j.jhydrol.2003.11.001

Koh, E. H., Lee, E., Kaown, D., Green, C. T., Koh, D. C., Lee, K. K., & Lee, S. H. (2018). Comparison of groundwater age models for assessing nitrate loading, transport pathways, and management options in a complex aquifer system. *Hydrological Processes*, *32*(7), 923–938. https://doi.org/10.1002/hyp.11465

Land, L., & Huff, G. F. (2010). Multi-tracer investigation of groundwater residence time in a karstic aquifer: Bitter Lakes National Wildlife Refuge, New Mexico, USA. *Hydrogeology Journal*, *18*(2), 455–472. https://doi.org/10.1007/s10040-009-0522-3

Lauber, U., & Goldscheider, N. (2014). Use of artificial and natural tracers to assess groundwater transit-time distribution and flow systems in a high-alpine karst system (Wetterstein Mountains, Germany). *Hydrogeology Journal*, *22*(8), 1807–1824. https://doi.org/10.1007/s10040-014-1173-6

Lehmann, B. E., Love, A., Purtschert, R., Collon, P., Loosli, H. H., Kutschera, W., … Gröning, M. (2003). A comparison of groundwater dating with ^{81}Kr, ^{36}Cl and ^{4}He in four wells of the Great Artesian Basin, Australia. *Earth and Planetary Science Letters*, *211*(3–4), 237–250. https://doi.org/10.1016/S0012-821X(03)00206-1

Long, A. J., & Putnam, L. D. (2009). Age-distribution estimation for karst groundwater: Issues of parameterization and complexity in inverse modeling by convolution. *Journal of Hydrology*, *376*(3–4), 579–588. https://doi.org/10.1016/j.jhydrol.2009.07.064

Lucas, L., & Unterweger, M. (2000). Comprehensive review and critical evaluation of the half-

life of tritium. *Journal of Research of the National Institute of Standards and Technology*, *105*(4), 541. https://doi.org/10.6028/jres.105.043

Maloszewski, P., & Zuber, A. (1982). Determining the turnover time of groundwater systems with the aid of environmental tracers. *Jounal of Hydrology, 57*, 207–231.

Mayer, A., Sültenfuss, J., Travi, Y., Rebeix, R., Purtschert, R., Claude, C., … Conchetto, E. (2014). A multi-tracer study of groundwater origin and transit-time in the aquifers of the Venice region (Italy). *Applied Geochemistry*, *50*, 177–198. https://doi.org/10.1016/j.apgeochem.2013.10.009

McMahon, P. B., Böhlke, J. K., & Christenson, S. C. (2004). Geochemistry, radiocarbon ages, and paleorecharge conditions along a transect in the central High Plains aquifer, southwestern Kansas, USA. *Applied Geochemistry*, *19*(11), 1655–1686. https://doi.org/10.1016/j.apgeochem.2004.05.003

Moral, F., Cruz-Sanjulián, J. J., & Olías, M. (2008). Geochemical evolution of groundwater in the carbonate aquifers of Sierra de Segura (Betic Cordillera, southern Spain). *Journal of Hydrology*, *360*(1–4), 281–296. https://doi.org/10.1016/j.jhydrol.2008.07.012

Mudarra, M., & Andreo, B. (2011). Relative importance of the saturated and the unsaturated zones in the hydrogeological functioning of karst aquifers: The case of Alta Cadena (Southern Spain). *Journal of Hydrology*, *397*(3–4), 263–280. https://doi.org/10.1016/j.jhydrol.2010.12.005

Müller, T., Osenbrück, K., Strauch, G., Pavetich, S., Al-Mashaikhi, K. S., Herb, C., … Sanford, W. (2016). Use of multiple age tracers to estimate groundwater residence times and long-term recharge rates in arid southern Oman. *Applied Geochemistry*, *74*, 67–83. https://doi.org/10.1016/j.apgeochem.2016.08.012

Musgrove, M., Solder, J. E., Opsahl, S. P., & Wilson, J. T. (2019). Timescales of water-quality change in a karst aquifer, south-central Texas. *Journal of Hydrology X*, *4*(July), 100041. https://doi.org/10.1016/j.hydroa.2019.100041

Palmer, A. N. (1984). Objectives and current status of alpine and arctic karst research. *Norsk Geografisk Tidsskrift*, *38*(3–4), 145–150. https://doi.org/10.1080/00291958408552118

Perrin, J., Jeannin, P. Y., & Zwahlen, F. (2003). Implications of the spatial variability of infiltration-water chemistry for the investigation of a karst aquifer: A field study at Milandre test site, Swiss Jura. *Hydrogeology Journal*, *11*(6), 673–686. https://doi.org/10.1007/s10040-003-0281-5

Plummer, L. N., Busby, J. F., Lee, R. W., & Hanshaw, B. B. (1990). Geochemical Modeling of the Madison Aquifer in Parts of Montana, Wyoming, and South Dakota. *Water Resources Research*, *26*(9), 1981–2014. https://doi.org/10.1029/WR026i009p01981

Poreda, R. J., Cerling, T. E., & Salomon, D. K. (1988). Tritium and helium isotopes as hydrologic tracers in a shallow unconfined aquifer. *Journal of Hydrology*, *103*(1–2), 1–9. https://doi.org/10.1016/0022-1694(88)90002-9

Rank, D., Volkl, G., Maloszewski, P., & Stichler, W. (1992). Flow dynamics in an alpine karst massif studied by means of environmental isotopes. *Isotope Techniques in Water Resources Development 1991. Proc. Symposium, Vienna, 1991*, 327–343.

Shah, R. A., Jeelani, G., & Jacob, N. (2017). Estimating mean residence time of karst groundwater in mountainous catchments of Western Himalaya, India. *Hydrological Sciences Journal*, *62*(8), 1230–1242. https://doi.org/10.1080/02626667.2017.1313420

Smart, C. C. (1988). Quantitative tracing of the Maligne karst system, Alberta, Canada. *Journal of Hydrology*, *98*(3–4), 185–204. https://doi.org/10.1016/0022-1694(88)90014-5

Solomon, D. K. (2000). ^{4}He in groundwater. In P.G. Cook & A. L. Herczeg (Eds.), *Environmental tracers in subsurface hydrology*. Springer Science+Business Media.

Solomon, D. K., Genereux, D. P., Plummer, L. N., & Busenberg, E. (2010). Testing mixing models of old and young groundwater in a tropical lowland rain forest with environmental tracers. *Water Resources Research*, *46*(4), 1–14. https://doi.org/10.1029/2009WR008341

Spangler, L. E. (2001). Delineation of Recharge Areas for Karst Springs in Logan Canyon ,. In E. L. Kumiansky (Ed.), *U.S. Geological Survey Karst Interest Group Proceedings, Water-Resources Investigations Report 01-4011* (pp. 186–193).

Stewart, M. K., & Thomas, J. . T. (2008). A conceptual model of flow to the Waikoropupu Springs, NW Nelson, New Zealand, based on hydrometric and tracer (O-18, Cl,H-3 and CFC) evidence. *Hydrology and Earth System Sciences*, *12*(1), 1–19. https://doi.org/10.5194/hess-12-1-2008

Stolp, B. J., Solomon, D. K., Suckow, A., Vitvar, T., Rank, D., Aggarwal, P. K., & Han, L. F. (2010). Age dating base flow at springs and gaining streams using helium-3 and tritium: Fischa-Dagnitz system, southern Vienna Basin, Austria. *Water Resources Research*, *46*(7), 1–13. https://doi.org/10.1029/2009WR008006

Suckow, A. (2014). The age of groundwater - Definitions, models and why we do not need this term. *Applied Geochemistry*, *50*, 222–230. https://doi.org/10.1016/j.apgeochem.2014.04.016

Sültenfuss, J., Purtschert, R., & Führböter, J. F. (2011). Age structure and recharge conditions of a coastal aquifer (northern Germany) investigated with ^{39}Ar, ^{14}C, ^{3}H, He isotopes and Ne. *Hydrogeology Journal*, *19*, 221–236. https://doi.org/10.1007/s10040-010-0663-4

Sültenfuss, J., Roether, W., & Rhein, M. (2009). The Bremen mass spectrometric facility for the

measurement of helium isotopes, neon, and tritium in water. *Isotopes in Environmental and Health Studies*, *45*(2), 83–95. https://doi.org/10.1080/10256010902871929

Torgersen, T., Clarke, W. B., & Jenkins, W. J. (1978). The tritium/helium-3 method in hydrology. In *Isotope Hydrology 1978, IAEA Symposium*. Neuherberg, Germany.

Toth, D. J., & Katz, B. G. (2006). Mixing of shallow and deep groundwater as indicated by the chemistry and age of karstic springs. *Hydrogeology Journal*, *14*(5), 827–847. https://doi.org/10.1007/s10040-005-0478-x

Turk, J., Malard, A., Jeannin, P. Y., Petrič, M., Gabrovšek, F., Ravbar, N., … Sordet, V. (2015). Hydrogeological characterization of groundwater storage and drainage in an alpine karst aquifer (the Kanin massif, Julian Alps). *Hydrological Processes*, *29*(8), 1986–1998. https://doi.org/10.1002/hyp.10313

USGS. (2018). Atmospheric mixing ratios of CFC-11, CFC-12, CFC-113, SF_6 x100, and tritium in precipitations for Northern Hemisphere atmosphere.

Visser, A., Broers, H. P., Purtschert, R., Sültenfuß, J., & de Jonge, M. (2013). Groundwater age distributions at a public drinking water supply well field derived from multiple age tracers (^{85}Kr, $^{3}H/^{3}He$, and ^{39}Ar). *Water Resources Research*, *49*(11), 7778–7796. https://doi.org/10.1002/2013WR014012

Werner, E. (1979). Alpine Karst in the Rocky Mountains. *Quarterly Journal of the National Speleological Society*, *41*(3), 51–52. https://doi.org/10.1017/CBO9781107415324.004

Wigley, T. M. L. (1973). The incongruent solution of dolomite. *Geochimica et Cosmochimica Acta*, *37*(5), 1397–1402. https://doi.org/10.1016/0016-7037(73)90072-0

Wilske, C., Suckow, A., Mallast, U., Meier, C., Merchel, S., Merkel, B., … Siebert, C. (2019). A

multi-environmental tracer study to determine groundwater residence times and recharge in a structurally complex multi-aquifer system. *Hydrology and Earth System Sciences Discussions*, (September), 1–30. https://doi.org/10.5194/hess-2019-451

Worthington, S. R. H., & Gunn, J. (2009). Hydrogeology of carbonate aquifers: A short history. *Ground Water*, *47*(3), 462–467. https://doi.org/10.1111/j.1745-6584.2008.00548.x

Wu, P., Shu, L., Li, F., Chen, H., Xu, Y., & Zou, Z. (2019). Impacts of Artificial Regulation on Karst Spring. *Water*, *11*, 755.

Xanke, J., Goeppert, N., Sawarieh, A., Liesch, T., Kinger, J., Ali, W., … Goldscheider, N. (2015). Impact of managed aquifer recharge on the chemical and isotopic composition of a karst aquifer, Wala reservoir, Jordan. *Hydrogeology Journal*, *23*(5), 1027–1040. https://doi.org/10.1007/s10040-015-1233-6

Xu, N., Gong, J., & Yang, G. (2018). Using environmental isotopes along with major hydro-geochemical compositions to assess deep groundwater formation and evolution in eastern coastal China. *Journal of Contaminant Hydrology*, *208*(November 2017), 1–9. https://doi.org/10.1016/j.jconhyd.2017.11.003

Yager, R. M., Plummer, L. N., Kauffman, L. J., Doctor, D. H., Nelms, D. L., & Schlosser, P. (2010). Comparison of age distributions estimated from environmental tracers by using binary-dilution and numerical models of fractured and folded karst : Shenandoah Valley of Virginia and West Virginia , USA. *Hydrogeology Journal*, *21*, 1193–1217. https://doi.org/10.1007/s10040-013-0997-9

Zang, H., Zheng, X., Qin, Z., & Jia, Z. (2015). A study of the characteristics of karst groundwater circulation based on multi-isotope approach in the Liulin spring area, North China. *Isotopes in Environmental and Health Studies*, *51*(2), 271–284.

https://doi.org/10.1080/10256016.2015.987275

Table 1. Statistical parameters of flow rate, electrical conductivity (EC), water temperature (Temp), major ion concentration, and ratio Mg/Ca (rMg/Ca) in the groundwater drained by the main springs of Jarastepar aquifer.

Spring/ Altitude (m a.s.l.)		**Flow rate** (l/s)	**EC** (µS/cm)	**Temp.** (°C)	**Alk** (mg/l)	**Ca^{2+}** (mg/l)	**Mg^{2+}** (mg/l)	**SO_4^{2-}** (mg/l)	**rMg/Ca**
Huertos 560	*n*	99	14735	16890	110	110	110	110	110
	min.	17.6	1747	16.3	214.0	387.3	75.6	991.7	0.11
	max.	32.9	1938	16.9	232.9	484.7	94.2	1309.2	0.13
	mean	**25.5**	**1875**	**16.7**	**226.4**	**437.3**	**87.0**	**1201.1**	**0.12**
	cv (%)	15.1	2.4	0.7	1.5	5.0	3.9	4.8	4.4
Charco 589	*n*	108	15164	15708	126	126	126	126	126
	min.	17.0	1550	15.6	203.7	343.5	58.7	892.3	0.09
	max.	29.7	1707	16.0	222.8	429.2	72.6	1165.1	0.11
	mean	**23.4**	**1673**	**15.8**	**211.2**	**396.1**	**66.0**	**1052.2**	**0.10**
	cv (%)	15.7	1.6	0.7	2.0	4.4	4.2	6.7	4.3
La Zúa 603	*n*	19754	8442	12436	126	126	126	126	126
	min.	149	1540	15.3	190.7	345.0	37.9	834.4	0.06
	max.	298	1591	16.0	226.0	451.4	50.9	1110.5	0.08
	mean	**208**	**1565**	**15.7**	**207.2**	**393.2**	**44.1**	**967.2**	**0.07**
	cv (%)	16.1	0.7	0.7	2.2	5.9	6.6	6.4	2.8
Overflow area 643-664	*n*	897†	19752	19752	198	198	198	198	198
	min.	0.1	260	13.6	165.4	49.6	1.4	1.7	0.02
	max.	21433	494	16.8	309.1	103.3	8.8	18.1	0.10
	mean	**2298**	**352**	**14.9**	**203.5**	**65.4**	**5.1**	**8.3**	**0.05**
	cv (%)	140.0	14.5	4.0	15.7	17.9	29.7	47.3	32.2

† The number of data of flow-rate in the overflow spring is lower than those of EC and Temp because it can only be measured in high water conditions.

Table 2. Environmental tracer data from the water samples collected at Jarastepar aquifer and derived groundwater date estimations.

Spring	Date of sample	System state	ΔNe (%)	^{3}H (TU)	$^{3}He_{trit}$ (TU)	$^{4}He_{rad}$ (ccSTP/kg)	CFC-12 (pmol/kg)	CFC-11 (pmol/kg)	SF_6 (pmol/kg)	CFC-12 (pptv)	CFC-11 (pptv)	SF_6 (pptv)	Tracer ages (years)		
													$^{3}H/^{3}He$	$^{4}He^{\dagger}$	CFC-12
La Zúa	25/10/14	IW	30.5	2.23	11.7	1.3E-5							33	66	
La Zúa	21/05/15	IW					1.58	2.28		295	111				36
La Zúa	29/08/15	LW	39.4	1.94	12	1.5E-5							35	75	
La Zúa	25/05/16	HW					1.30		0.22	243		601			41
La Zúa	09/12/16	HW	34.9	1.74	11.9	1.6E-5							36	78	
Charco	25/10/14	IW	27.0	2.46	15.7	2.0E-5							36	101	
Charco	21/05/15	IW					1.04	1.53		195	75				42
Charco	29/08/15	LW	34.5	2.06	16.8	2.2E-5							40	110	
Charco	25/05/16	HW					1.11		0.22	209		593			42
Charco	09/12/16	HW	26.9	1.9	13.2	1.8E-5							37	92	
Huertos	25/10/14	IW	28.4	2.1	11.6	2.6E-5							33	131	
Huertos	21/05/15	IW					0.98	1.27		184	62				42
Huertos	29/08/15	LW	30.7	1.74	12.6	2.3E-5							38	115	
Huertos	25/05/16	HW					0.99		0.17	184		453			43
Huertos	09/12/16	HW	27.7	1.65	10.4	2.6E-5							35	129	

LW, IW, and HW refer to low, intermediate and high water hydrodynamic situations. †Ages calculated assuming a $^{4}He_{rad}$ dissolution rate of $2 \cdot 10^{-7}$ ccSTP·kg^{-1}·yr^{-1}, according to the results of the Lumped Parameter Models.

Table 3. Characteristics of the bins included in the Shape-Free Models (years).

5-bin model	Bin 1	Bin 2	Bin 3	Bin 4	Bin 5 (old bin)
Age range	0-20	20-40	40-60	60-80	80-160 (78-200) †
Mean age	10	30	50	70	120 (140) †
^{3}H (TU)	2.10	1.64	8.64	0.18	0
$^{3}He_{trit}$ (TU)	2.5	14.9	101.6	6.9	0
CFC-12 (pptv)	537.2	415.0	98.9	5.7	0
$^{4}He_{rad}$ (ccSTP/kg)	2.1E-6	6.1E-6	1.0E-5	1.4E-5	2.4E-5
4-bin model	**Bin 1**	**Bin 2**	**Bin 3**	**Bin 4 (old bin)**	
Bin range	0-26	26-52	52-78	78-160 (78-200) †	
Mean age	13	39	65	119 (136) †	
^{3}H (TU)	1.95	4.15	3.56	0	
$^{3}He_{trit}$ (TU)	5.17	37.86	63.53	0	
CFC-12 (pptv)	533.49	263.473	15.84	0	
Mean age	13	39	65	119 (136) †	

† Values in brackets are referred only to samples from Huertos spring.

Table. 4. Results from groundwater distribution age models. BMM, Binary Mixing Model; PFM, Piston Flow Model; DM, Dispersion Model, SFM, Shape-Free Model; RMSE, Root of the Mean Square Error.

Spring	Date of sample	Sample				BMM (PFM-PFM)			BMM (DM-DM)					5-bin SFM			4-bin SFM	
		^{3}H (TU)	$^{3}He_{trit}$ (TU)	$^{4}He_{rad}$ (ccSTP/kg)	CFC-12 (pptv)	F_{young} (%)	F_{old} (%)	F_{young} age	Mean age (years)	F_{young} (%)	F_{young} age	F_{old} age	GA_{50} (years)	Mean age (years)	GA_{50} (years)	Old Bin (%)	GA_{50} (years)	Old Bin (%)
La Zúa	25/10/2014	2.23	11.67	1.3E-05	295	100	0	33	69	68	25	160	30	54	20	0	52	32
La Zúa	09/12/2016	1.74	11.90	1.6E-05	243	87	13	36	85	57	27	160	38	65	60	26	52	41
Charco	25/10/2014	2.46	15.66	2.0E-05	195	70	30	38	93	52	31	160	47	77	>80	52	>72	44
Charco	09/12/2016	1.90	13.20	1.8E-05	209	69	31	37	93	51	29	160	46	75	80	0	>72	45
Huertos	25/10/2014	2.10	11.66	2.6E-05	184	58	42	38	119	48	29	200	66	94	>80	57	>78	51
Huertos	09/12/2016	1.65	10.40	2.6E-05	184	56	44	37	123	45	29	200	77	95	80	0	>78	53

Table 5. P-values between physicochemical and groundwater-age parameters. Italics and bold figures show non-significant correlations for confidence intervals of 95% and 90%, resepctively. BMM, Binary Mixing Model; PFM, Piston Flow Model; DM, Dispersion Model, SFM, Shape-Free Model.

	Perecentage of F_{old}			Mean age				Median Age
	PFM-PFM	DM-DM	FSM (4-bin)	PFM-PFM	DM-DM	FSM (4-bin)	FSM (5-bin)	DM-DM
Electrical conductivity	0.033	*0.082*	0.035	0.037	0.008	0.005	0.008	0.011
Water temperature	*0.058*	0.123	*0.055*	*0.065*	0.014	0.012	0.017	0.016
SO_4	**0.169**	**0.303**	**0.221**	**0.175**	**0.128**	*0.097*	*0.103*	**0.158**
Mg/Ca	0.001	0.015	0.008	0.002	0.005	0.004	0.002	0.006

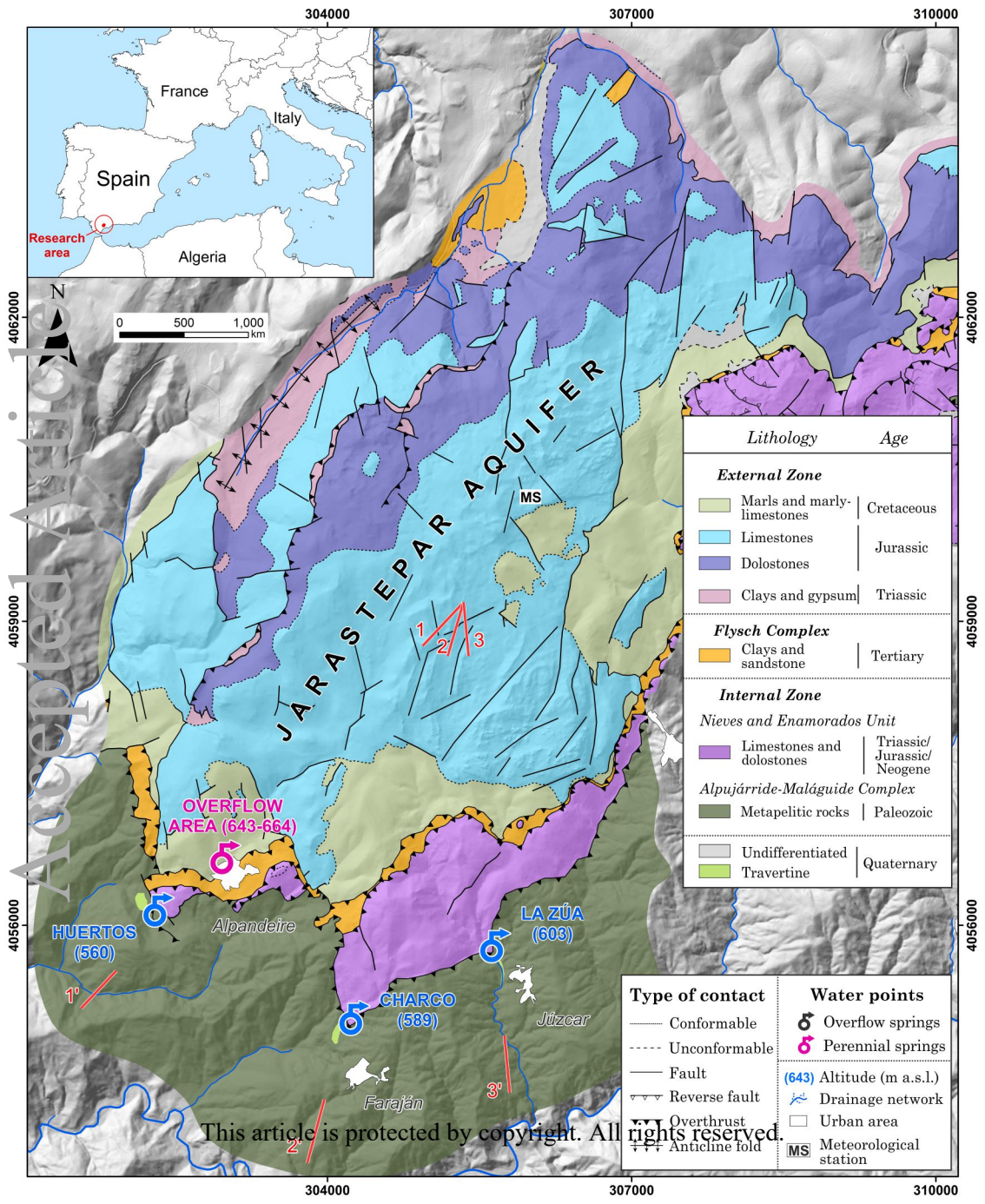

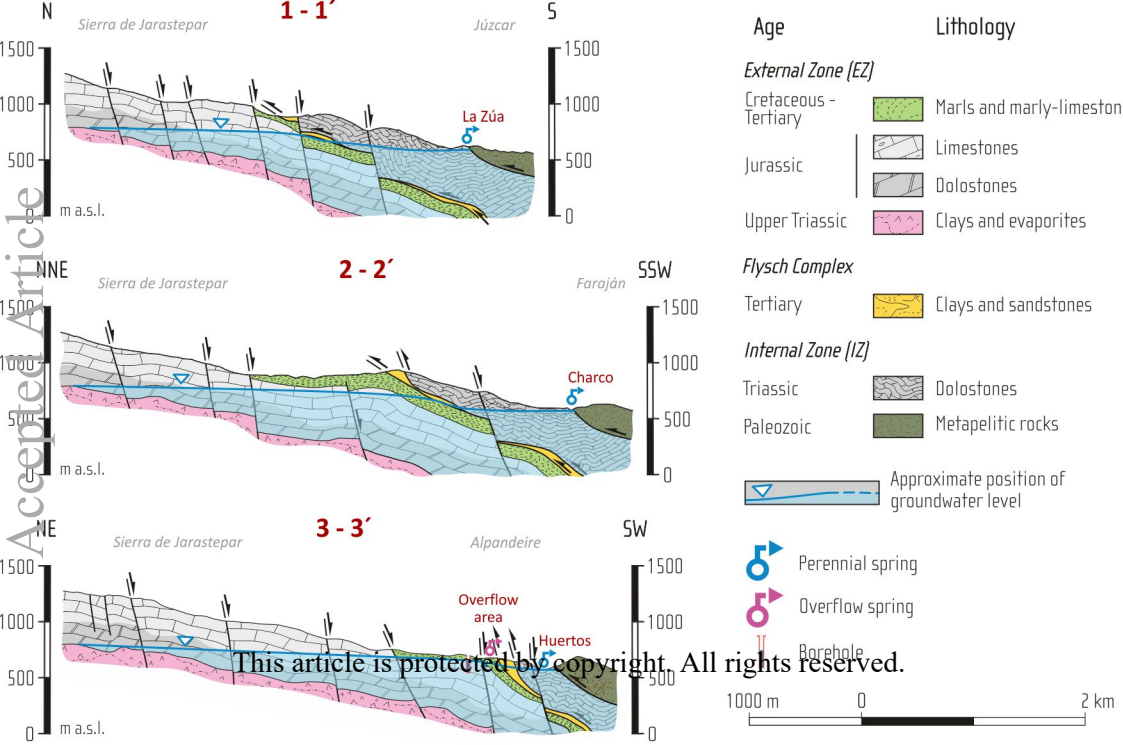

2014 2015 2016

Oct Dec Feb Apr Jun Aug Oct Dec Feb Apr Jun Aug Oct Dec

IW IW LW HW HW

³H-He sampling

CFC sampling

Huertos
Charco
La Zúa
Overflow

Piezometric level

Rainfall (mm/day)

Piezometric level (m a.s.l.)

Discharge (l/s)

EC (µS/cm)

Temperature (ºC)

SO_4^{2-} (mg/l)

Mg^{2+} (mg/l)

Ca^{2+} (mg/l)

Spring
max.
P_{75}
mean
P_{25}
min.

Overflow La Zúa Charco Huertos

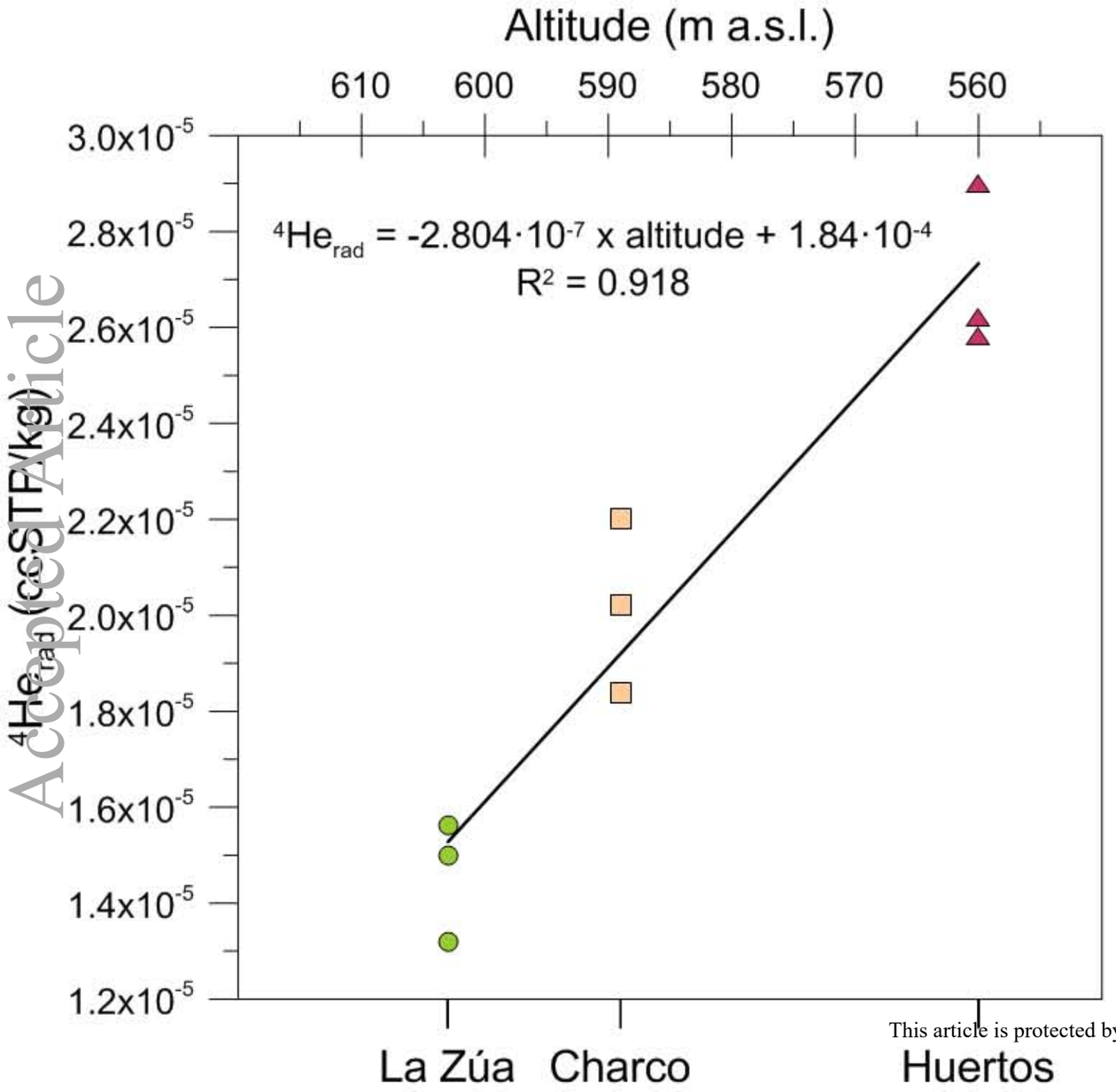

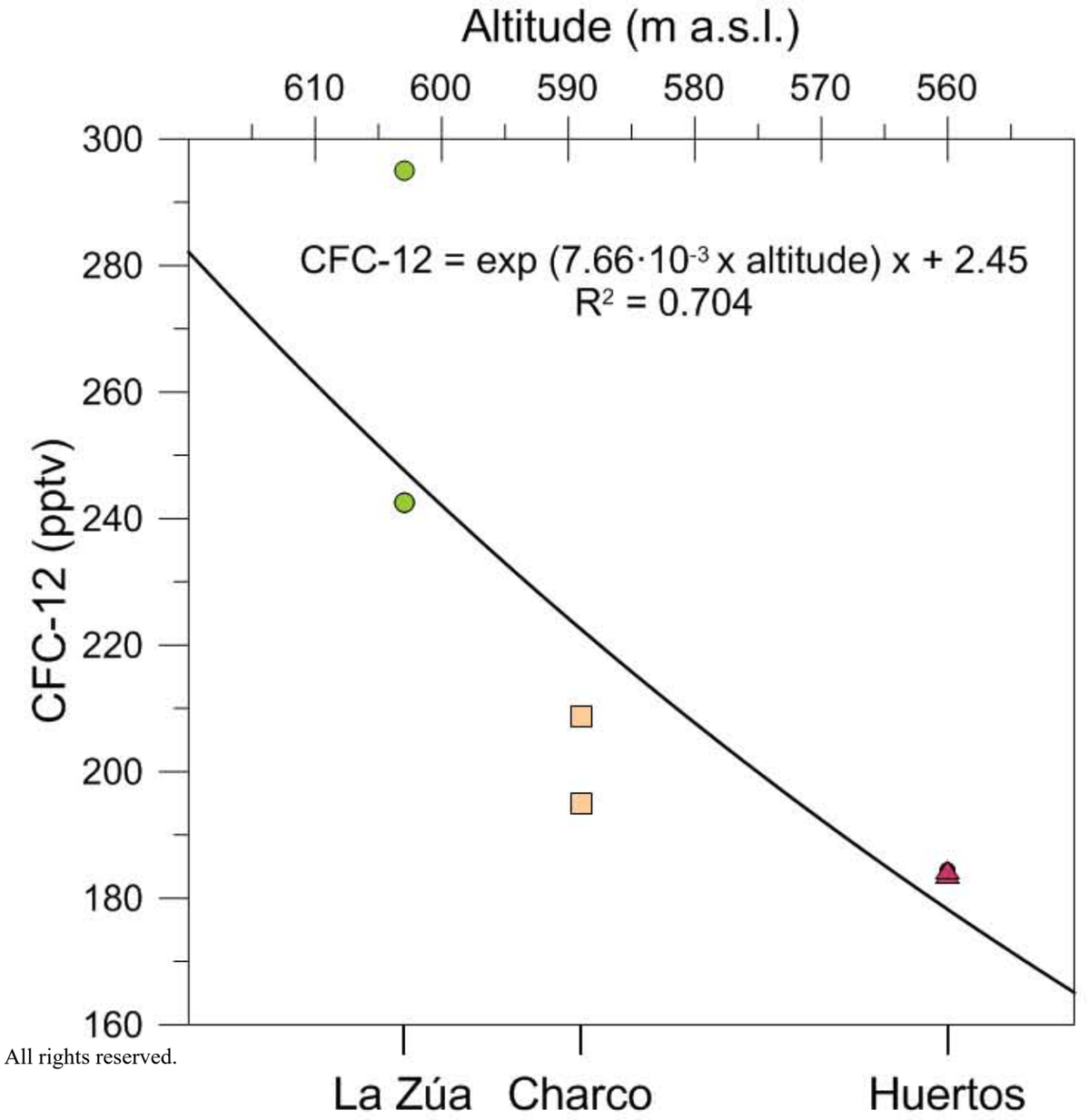

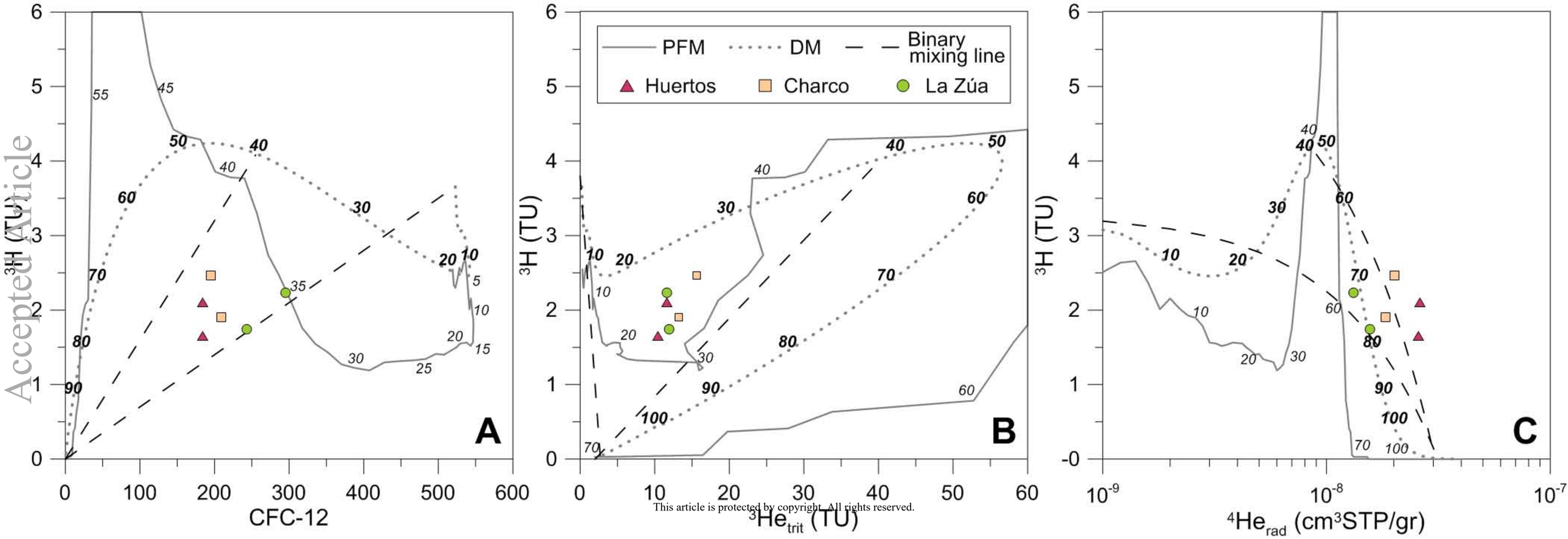

La Zúa 25/10/2014
Charco 25/10/2014
Huertos 25/10/2014
50% of cumulative fraction
La Zúa 09/12/2016
Charco 09/12/2016
Huertos 09/12/2016